A Predictive Model for Transient Enhanced Diffusion Based on Evolution of {311} Defects

Alp H. Gencer and Scott T. Dunham
Department of Electrical and Computer Engineering
Boston University, Boston, MA 02215
http://engc.bu.edu/~alp

Submitted to **Journal of Applied Physics**, *September 1996.*

It has been observed that {311} defects form, grow and eventually dissolve during annealing of Si implanted silicon wafers. The fact that for sub-amorphizing silicon implants {311} defects initially contain the full net dose of excess interstitials, and that the time scale for dissolution of these defects is about the same as the time scale of transient enhanced diffusion (TED), leads to the conclusion that {311} defects are a primary source of interstitials under TED conditions. In this paper, we describe a comprehensive model which accounts for the evolution of these defects during ion implant annealing; and in combination with point defect parameters from previous work, also correctly predicts TED behavior.

1. INTRODUCTION

Transmission Electron Microscopy (TEM) observations[1,2] show that {311} defects (also known as "rod-like defects") form, grow and eventually dissolve during annealing of ion implanted samples. Initially, there is a huge driving force to form {311} defects, such that, for sub-amorphizing silicon implants, almost the whole net excess interstitial dose aggregates into these extended defects within a very short period of time (less than 5 s at 815°C).[1] As annealing continues, these defects undergo Ostwald ripening: Their average size increases and their number decreases. The total number of interstitials bound to these defects decreases approximately exponentially, and eventually, all {311} defects dissolve and disappear. It has been reported that the time scale for their dissolution is about the same as the time scale of TED.[2] These observations strongly suggest that {311} defects play a central role under TED conditions. If we could model the evolution of these defects correctly, we should be able to predict TED. Indeed, we have developed a comprehensive model for the evolution of {311} defects during annealing of sub-amorphizing Si implants and used this model to correctly predict TED and its dependence on implant and anneal conditions.

2. THE MODEL

To model the evolution of {311} defects, we have applied the Kinetic Precipitation Model[3] to interstitials. The model was initially used for the modeling of dopant precipitation, but can be adopted to the evolution of {311} defects, since these defects can be viewed as precipitates formed by interstitial silicon atoms. The major challenge in modeling the evolution of precipitates and extended defects is the fact that different sized defects have very different properties. The kinetic precipitation model treats precipitates of different sizes as independent species (f_n) and accounts for their kinetics by considering the attachment and emission of solute atoms.

The driving force for precipitation, or in this case {311} defect formation, is the minimization of the free energy of the system, where the free energy of a size n extended defect is given by:

$$\Delta G_n = -nkT \ln \frac{C_{\rm I}}{C_{\rm ss}} + \Delta G_n^{\rm exc} \tag{1}$$

Here, $C_{\rm ss}$ is the "solid solubility" of interstitials associated with the formation of {311} defects and $\Delta G_n^{\rm exc}$ is the excess surface and strain energy of a size n extended defect. We have assumed that $\Delta G_n^{\rm exc}$ has a polynomial form:

$$\Delta G_n^{\rm exc} = a_0 n^{\beta_0} + a_1 n^{\beta_1} \tag{2}$$

with $\beta_1 < \beta_0 < 1$. Theoretical calculations[4] for the functional form of $\Delta G_n^{\rm exc}$ show that it is reasonable to assume that $\beta_0 = 0.5$ since {311} defects are planar defects. We used $\beta_1 = -0.5$ as a correction for small size behavior. The coefficients a_0 and a_1 remain as temperature independent fitting parameters.

Kinetics of the model

The main reaction in the system is the attachment and emission of interstitials to and from the extended defects. If I_n denotes the net growth rate from size n to $n+1$ we may write the following equation:

$$I_n = \begin{cases} D_{\rm I}\lambda_n \left(C_{\rm I} f_n - C_n^* f_{n+1}\right) & \text{for } n \geq 2 \\ D_{\rm I}\lambda_1 \left({C_{\rm I}}^2 - C_1^* f_2\right) & \text{for } n = 1 \end{cases} \tag{3}$$

Note that I_1 is different from other terms, because it represents the rate for formation of the defects by reaction of two interstitials.

The growth rate of {311} defects is written in the form $D_{\rm I}\lambda_n$, where λ_n incorporates effects of both diffusion to the precipitate/silicon interface and the reaction at the interface. λ_n is calculated based on solving the steady-state diffusion equation in the neighborhood of an elongated planar defect, such as a {311} defect. A detailed analysis and derivation is given in the Appendix. C_n^* represents the interstitial concentration at which a size n defect would gain no energy by growing from size n to size $n+1$:

$$C_n^* = C_{\rm ss} \exp\left(\frac{\Delta G_{n+1}^{\rm exc} - \Delta G_n^{\rm exc}}{kT}\right) \tag{4}$$

The evolution of the size distribution f_n is given by the difference between the net rate at which defects grow from size $n-1$ to n (I_{n-1}) and the net rate of growth from size n to $n+1$ (I_n). Since the fundamental growth process is the incorporation of an interstitial, the total change in $C_{\rm I}$ includes a term from each growth reaction, giving a sum over I_n:

$$\frac{\partial f_n}{\partial t} = I_{n-1} - I_n \tag{5}$$

$$\frac{\partial C_{\rm I}}{\partial t} = -2I_1 - \sum_{n=2}^{\infty} I_n \tag{6}$$

Reduced Precipitation Model

To integrate the Kinetic Precipitation Model into a diffusion equation solver, Clejan and Dunham[5] have developed a more efficient version of this model. Instead of calculating all the f_n, one needs to calculate only the lowest three *moments* of the distribution ($m_i = \sum_{n=2}^{\infty} n^i f_n$, where $i = 0, 1, 2$) and make a closure assumption. In particular, the closure assumption used is that the distribution is the one that minimizes the free energy, given the moments. The resulting system, when applied to {311} defects has the following set of continuity equations:

$$
\begin{aligned}
\frac{\partial m_0}{\partial t} &= I_1 \\
\frac{\partial m_1}{\partial t} &= 2I_1 + \sum_{n=2}^{\infty} I_n \\
\frac{\partial m_2}{\partial t} &= 4I_1 + \sum_{n=2}^{\infty} I_n(2n+1) \\
\frac{\partial C_\mathrm{I}}{\partial t} &= D_\mathrm{I}\nabla^2 C_\mathrm{I} - k_\mathrm{R}(C_\mathrm{I}C_\mathrm{V} - C_\mathrm{I}^*C_\mathrm{V}^*) - 2I_1 - \sum_{n=2}^{\infty} I_n \\
\frac{\partial C_\mathrm{V}}{\partial t} &= D_\mathrm{V}\nabla^2 C_\mathrm{V} - k_\mathrm{R}(C_\mathrm{I}C_\mathrm{V} - C_\mathrm{I}^*C_\mathrm{V}^*)
\end{aligned}
\tag{7}
$$

Note that the sums over the I_n can all be written in terms of sums over f_n and nf_n, and hence can be calculated from the three moments.[5] However, these calculations require the solution of a non-linear equation system at every time step and each grid point. To make the simulation computationally efficient, the sums are pre-tabulated for a range of m_i values and interpolation from these values is used during the simulation.

3. PARAMETERS

Under TED conditions, the surface is the main sink for interstitials. Data by Eaglesham *et al.*[1] suggest a surface recombination rate that is decreasing with time, since the rate at which interstitials are consumed is decreasing approximately exponentially with time. Other experimental observations also indicate that a fast effective interstitial surface regrowth exists for small thermal budgets, with a much slower one for longer times and higher temperatures.[6] Thus, rather than using a simple model with constant surface recombination rate, we used the film segregation model of Agarwal and Dunham[7] to account for surface regrowth. In this model, the primary mechanism by which the surface consumes interstitials is not surface recombination, but segregation of interstitials to the oxide layer. We use their parameters without any modification.

For bulk point defect parameters (diffusivities and equilibrium concentrations of interstitials and vacancies), we use the values calculated from metal diffusion (Zn, Au and Pt).[8,9] We furthermore assume that both I/V recombination and interstitial precipitation are diffusion limited. The kinetic rate for precipitation for {311} defects (λ_1) is calculated in a similar manner to Dunham,[10] but accounting for the rod-like defect shape, as given in the Appendix. Initial defect profiles are calculated from Monte-Carlo simulations using TRIMCSR and UT-MARLOWE. The system has been implemented in PEPPER[11] and DOPDEES (Dial-an-Operator Partial Differential Equation Evaluator and Solver).[12]

4. EVOLUTION OF {311} DEFECT PROFILE

Eaglesham *et al.*[1] implanted $5 \times 10^{13}\,\mathrm{cm}^{-2}$ Si into silicon at 40 keV and annealed the samples at 815°C and 670°C. They measured the resulting {311} defect distributions using TEM and reported the moments of this distribution. We optimized our parameters (a_0, a_1 and C_{ss}, with only C_{ss} being temperature dependent) to match just the evolution of the number of interstitials in these defects (m_1). It can be seen that we were able to obtain a good agreement between the data and the model (Fig. 1). Although we did not optimize the parameters to match the size evolution, the model gave a good prediction for the observed Ostwald ripening behavior (Fig. 2).

To gain a better understanding of the system, we can examine the relationship between the Ostwald ripening behavior and the exponential decay of m_1. Fig. 3 shows a plot of C_n^* versus defect size for this system. As the defect size increases, the interstitial concentration that is in equilibrium with the {311} defects decreases. This decreases the gradient and thus the flux of interstitials from the region with {311} defects to the surface, resulting in a decrease in the rate at which the interstitials are consumed. If we examine how the depth profile changes over time (Fig. 4), we observe that the {311} defect profile is consumed from the side that is closer to the surface, and this process moves the profile frontier deeper into the substrate with time, again reducing the interstitial gradient towards the surface. Thus, the approximately exponential decay of the number of interstitials in {311} defects arises from a combination of the time-varying effective surface regrowth velocity, the Ostwald ripening behavior, and the shift of the {311} defect frontier away from the surface. As also seen in the work of Rafferty *et al.*,[13] models that do not take the Ostwald ripening process into account and have fixed surface recombination velocity result in a rate of decrease in m_1 that is closer to linear than exponential.

We applied the same system and parameters to the dose dependence of interstitials in {311} defects. Poate *et al.*[14] reported that above a threshold dose the number of interstitials in {311} defects at the initial stages of TED increases approximately linearly with implant dose, but with a slope of about 1.4. As shown in Fig. 5, our model accurately predicts this behavior, both the slope as well as the dose below which no {311} defects were observed ($5 \times 10^{12}\,\mathrm{cm}^{-2}$).

5. PREDICTION OF TED

We used the parameters obtained in the previous section to predict TED behavior as a function of implant and annealing conditions. For comparison, we used data from Packan,[15] who implanted ^{29}Si into silicon at energies ranging from 10 keV to 200 keV and doses ranging from 1×10^{12} to $2 \times 10^{14}\,\mathrm{cm}^{-2}$. TED was measured by observing profile movement of an intrinsic boron marker layer. No further fitting was done at this stage and all parameters were from work cited previously[7,8] or from matching the data for {311} defect evolution (Fig 1).

Our results show that the model does a good job in predicting the magnitude of TED, as well its dependence on implant energy and dose and annealing temperature and time (Figs. 6–9). It is evident that the total amount of TED increases with increasing implant energy (Fig. 6). Although the enhancements for different implant energies are similar during the initial stages of TED, for higher energies TED lasts longer, increasing the total profile movement (Fig. 7). The reason for this behavior is that at higher implant energies, the implanted profile is further away from the surface, so that the interstitial gradient towards the surface is smaller.

The model also predicts the dose dependence correctly, with the exception of the very lowest dose (Figs. 8 and 9). It may be noted that the strong sub-linear dose dependence of TED for very low doses seen in the experimental results is in apparent contradiction with the observed linear dependence of the number of interstitials in {311} defects on dose.[14] As with changes in implant energy, different doses give similar enhancements for short times, but TED lasts longer at higher doses (Fig. 9). The observed time dependence arises because the higher dose results in a correspondingly larger number of excess interstitials in the substrate, while the flux towards the surface is nearly independent of dose since the free interstitial concentration is controlled by the {311} defects.

6. CONCLUSIONS

In summary, we were able to match the evolution of {311} defects using a model that is based on the evolution of the lowest three moments of the extended defect population, and used this model to predict the dependence of TED on implant and annealing conditions. The model relies on the fundamental physical processes occurring under TED conditions. The advantage of using such a model is the potential for extension to simulation of experimental conditions that are different from which the model was tested and calibrated on. The power of this approach is illustrated by both the relatively small number of fitting parameters to get good agreement with the {311} defect evolution data and the good predictions for defect size evolution, dose dependence and TED behavior.

This work was supported by the Semiconductor Research Corporation.

APPENDIX A: Calculation of the kinetic growth rate ($D_{\mathrm{I}}\lambda_n$) for {311} defects

To calculate the kinetic growth rate of {311} defects, we solved for the steady-state diffusion field around a {311} defect, calculating the flux at the interface following the technique used by Dunham.[10] We assumed that {311} defects are planar with a rectangular shape and grow primarily in their length.[16] The capture cross-section of a {311} defect is assumed to be cylindrical regions of radius b with half-spheres at each end (Fig. 10), where b is the silicon lattice spacing. In order to find the diffusion field around a {311} defect, we divided this region into spheres of radius b which have a total surface area equal to that of the sum of the two cylinders and four half-spheres. We then added up the steady-state diffusion fields of these spheres to find the concentration at a distance r along the mid-line of the width of a {311} defect:

$$\begin{aligned}\tilde{C}(r) &= 2\sum_{i=1}^{N/2}\frac{c^s b}{\sqrt{r^2+(iw/N)^2}} + 2\sum_{i=1}^{N/2}\frac{c^s b}{\sqrt{(l+r)^2+(iw/N)^2}} \\ &= 4c^s\left[\ln\left(w/2+\sqrt{r^2+(w/2)^2}\right) - \ln(r) + \ln(w/2+\sqrt{(l+r)^2+(w/2)^2}) - \ln(l+r)\right]\end{aligned} \tag{8}$$

where $\tilde{C}$ denotes normalized concentrations ($C - C^{\infty}$, with C^{∞} being the concentration of interstitials far away from the extended defect), c^s is the normalized concentration at the surface of each sphere, $N = w/2b + 1$ is the number of spheres on either end of the {311} defect, and w and l are the width and the length of the {311} defect, respectively.

The kinetic precipitation rate can be calculated from the solution of the boundary condition for the flux:

$$A_n D \left.\frac{d\tilde{C}}{dr}\right|_{r=\mathrm{surface}} = A_n k(\tilde{C}_n^{\mathrm{int}} - \tilde{C}_n^*) \tag{9}$$

where $\tilde{C}_n^{\rm int}$ denotes the normalized concentration at the interface, $\tilde{C}_n^*$ denotes the normalized concentration that would be in equilibrium with a size n precipitate, $A_n = 4\pi bw + 8\pi b^2$ is the total area of the two cylinders and four hemi-spheres, and k is the surface reaction rate. Substituting (8) into (9) gives:

$$\left.\frac{d\tilde{C}}{dr}\right|_{r=\rm surface} = -\frac{\tilde{C}_n^{\rm int}}{R^{\rm eff}} \tag{10}$$

where

$$R^{\rm eff} = \frac{\left[\ln\left(1+\sqrt{1+(2b/w)^2}\right) - \ln(2b/w) + \ln\left(1+\sqrt{1+(2(l+b)/w)^2}\right) - \ln(2(l+b)/w)\right]}{\left[\dfrac{1}{b\sqrt{1+(2b/w)^2}} + \dfrac{1}{(l+b)\sqrt{1+(2(l+b)/w)^2}}\right]} \tag{11}$$

This gives the kinetic precipitation rate to be[10]

$$D_{\rm I}\lambda_n = \frac{D_{\rm I}A_n}{R^{\rm eff} + D_{\rm I}/k} \tag{12}$$

$D_{\rm I}\lambda_n$ is the effective reaction rate at the Si/defect interface, taking both actual surface recombination and diffusivity into account.

Since our model uses n, the number of interstitials in {311} defects, as a parameter, we need a relationship between n, w and l. The density of interstitials in {311} defects is known[16] to be $5\times10^{14}\,\rm cm^{-2}$, but the relation between w and l is unknown. It has been observed[1,17] that {311} defects have a maximum average width of about 5 nm, but it would be unreasonable to assume that their width is always 5 nm, thus larger than their length for $l < 5$ nm. We therefore assume that the width may be expressed by $w = \min(l, 5\,\rm nm)$. This assures that $l \geq w$ and $w = 5$ nm for large sizes which can be observed under HRTEM. Other functions with similar characteristics can also be used, but have no significant effect on λ_n.

---

[1] D.J. Eaglesham, P.A. Stolk, H.J. Gossmann, and J.M. Poate, *Appl. Phys. Lett.* **65**, 2305 (1994).

[2] N.E.B. Cowern, G.F.A. van de Walle, P.C. Zalm, and D.W.E. Vandenhoudt, *Appl. Phys. Lett.* **65**, 2981 (1994).

[3] S.T. Dunham, *J. Electrochem. Soc.* **142**, 2823 (1995).

[4] A. Parisini and A. Bourret, *Phil. Mag. A* **67**, 605 (1993).

[5] I. Clejan and S.T. Dunham, *J. Appl. Phys.* **78**, 7327 (1995).

[6] S.T. Dunham and A.M. Agarwal, in **ULSI Science and Technology**, 235 (1995).

[7] A.M. Agarwal and S.T. Dunham, *J. Appl. Phys.* **78**, 5313 (1995).

[8] H. Bracht, N.A. Stolwijk, and H. Mehrer, *Phys. Rev. B* **52**, 16542 (1995).

[9] H. Zimmermann and H. Ryssel, *Applied Physics A* **55**, 121 (1992).

[10]S.T. Dunham, *Appl. Phys. Lett.* **63**, 464 (1993).

[11]B.J. Mulvaney, W.B. Richardson, and T.L. Crandle, *IEEE Trans. Comp. Aided Des.* **8**, 336 (1989).

[12]A.H. Gencer. *DOPDEES User's Manual* (1996).

[13]C.S. Rafferty, G.H. Gilmer, M. Jaraiz, D. Eaglesham, and H.J. Gossmann, *Appl. Phys. Lett.* **68**, 2395 (1996).

[14]J.M. Poate, D.J. Eaglesham, and G.H. Gilmer, in **IEDM Technical Digest**, 77 (1995).

[15]P.A. Packan, PhD thesis, Stanford University (1991).

[16]S. Takeda, M. Kohyama, and K. Ibe, *Phil. Mag. A* **70**, 28 (1994).

[17]K.S. Jones, J. Lui, L. Zhang, V. Krishnamoorthy, and R.T. DeHoff, *Nuc. Inst. and Meth. B* **106**, 227 (1995).

Parameter	Pre-exp.	Activation	Source
D_{I} (cm^2/s)	5.1×10^1	1.77	Bracht[8]
D_{V} (cm^2/s)	3.0×10^{-2}	1.80	Bracht[8]
C_{I}^* (cm^{-3})	2.9×10^{24}	3.18	Bracht[8]
C_{V}^* (cm^{-3})	1.4×10^{24}	2.00	Bracht[8]
$D_{\mathrm{I}}^{\mathrm{SiO_2}}$ (cm^2/s)	1.3×10^1	4.50	Agarwal[7]
m_{seg}	1.24	-2.11	Agarwal[7]

Table 1: Point defect parameters used in this work. $D_{\mathrm{I}}^{\mathrm{SiO_2}}$ is the diffusivity of interstitials (excess silicon) in SiO_2 and m_{seg} is the equilibrium segregation coefficient for interstitials between Si and SiO_2.

Parameter	Pre-exp.	Activation
a_0 (eV)	1.76	–
a_1 (eV)	1.39	–
C_{ss} (cm^{-3})	7.7×10^{22}	2.22

Table 2: $\{311\}$ defect parameters extracted from matching the evolution of the total number of interstitials in $\{311\}$ defects (m_1).

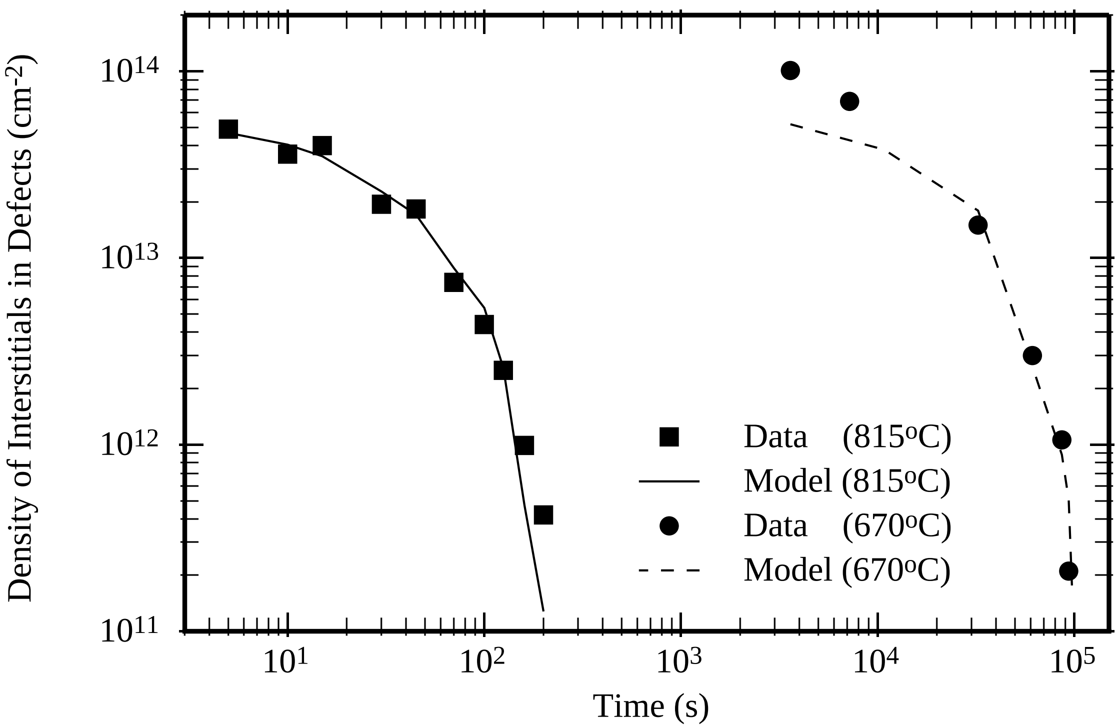

Fig. 1: Evolution of density of interstitials in $\{311\}$ defects (m_1) and comparison to model. Data from Eaglesham *et al.*[1] for $5 \times 10^{13}\,\mathrm{cm}^{-2}$ Si implants at 40 keV with anneals at 815°C and 670°C.

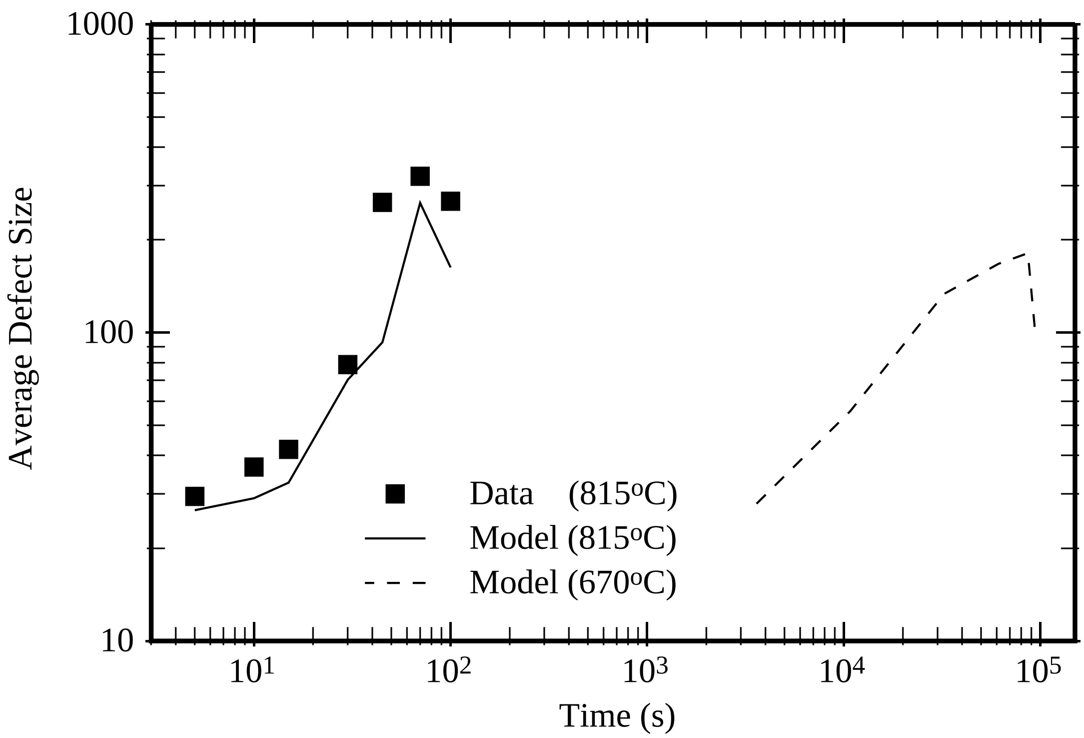

Fig. 2: Prediction of evolution of average defect size (m_1/m_0) during annealing of $5 \times 10^{13}\,\mathrm{cm}^{-2}$ Si implants at 40 keV and comparison to data from Eaglesham *et al.*[1]

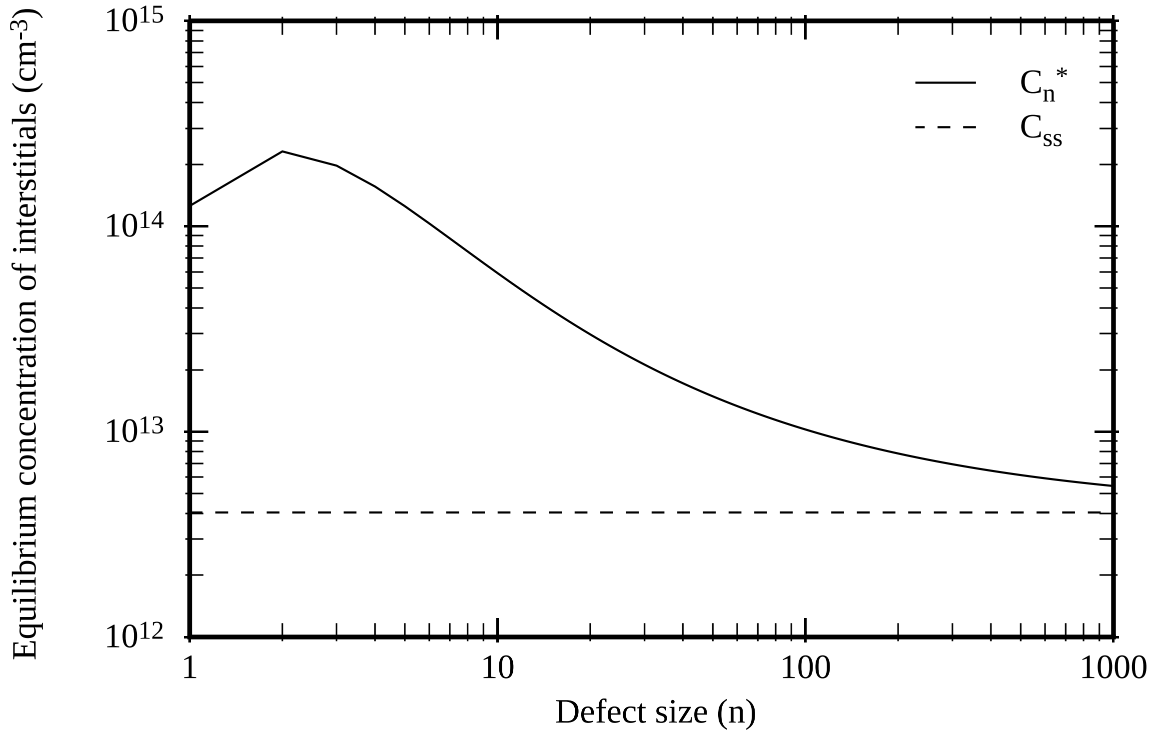

Fig. 3: The concentration of interstitials at equilibrium with {311} defects as a function of defect size for anneals at 815°C.

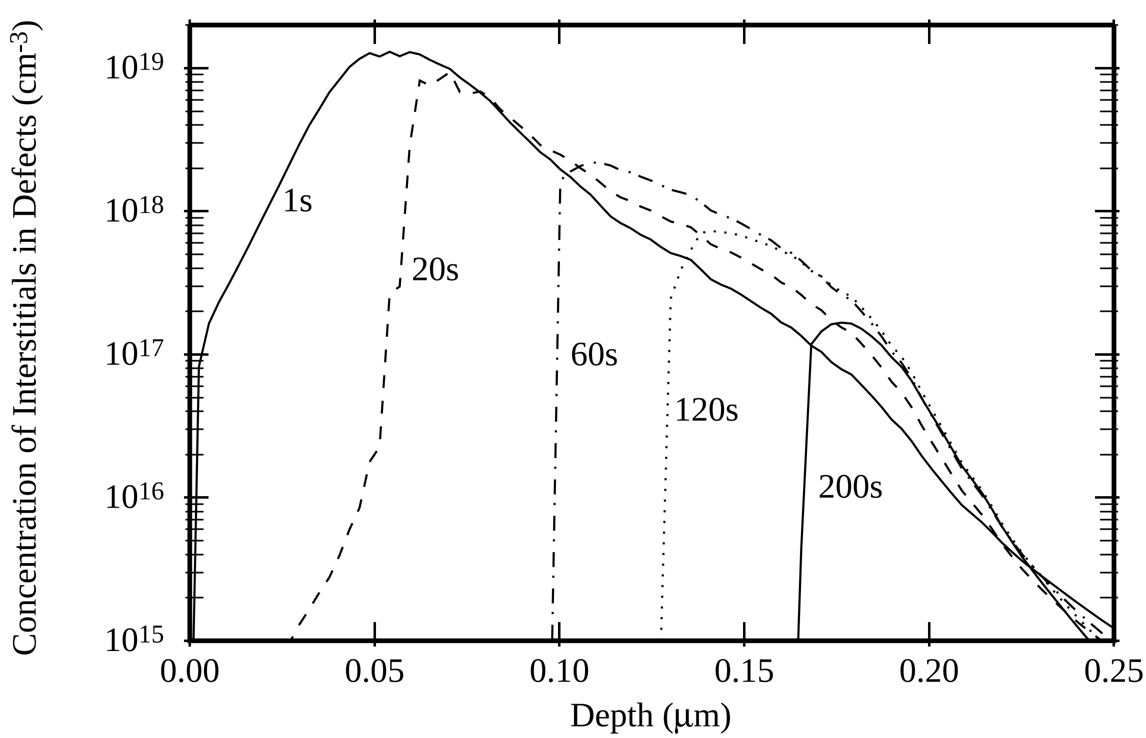

Fig. 4: Simulated {311} defect profiles for various annealing times at 815°C.

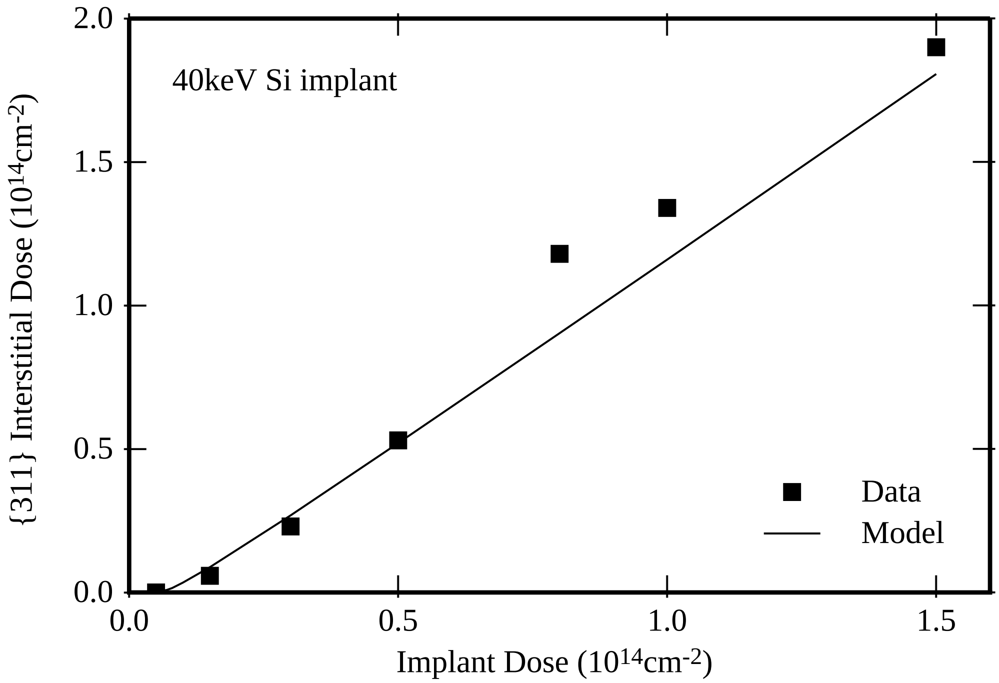

Fig. 5: Prediction of dose dependence of interstitials in {311} defects during initial stages of TED. Data from Poate *et al.*[14] for 40 keV Si implants and 1 h anneal at 670°C.

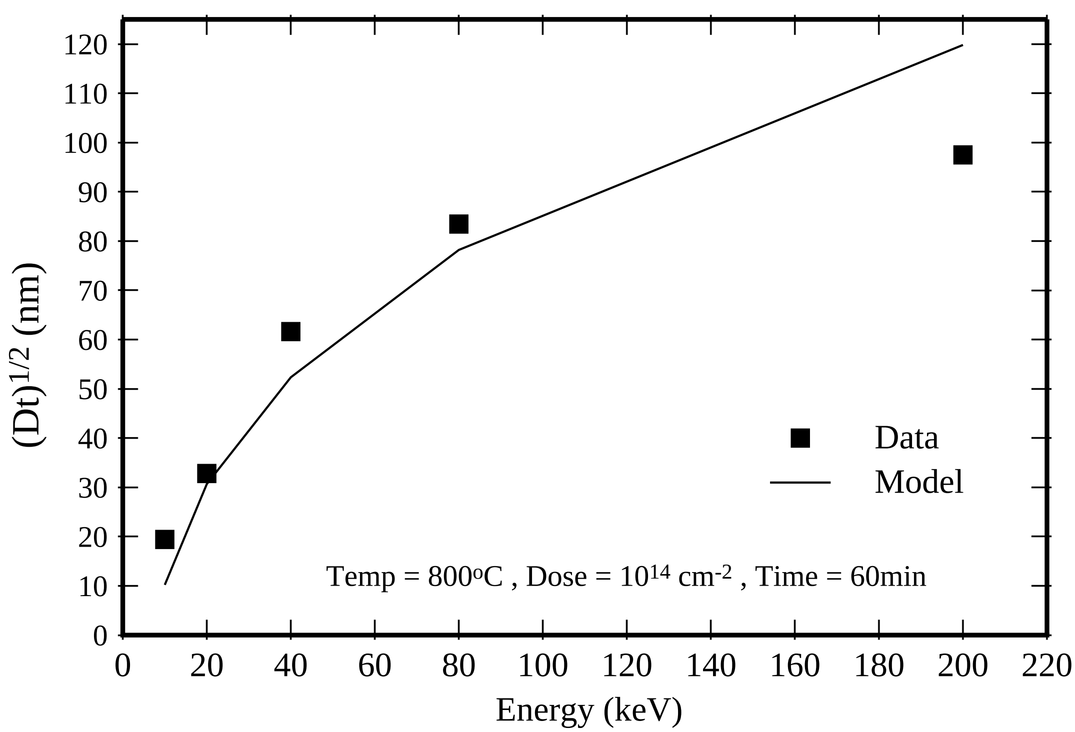

Fig. 6: Energy dependence of TED. Total broadening of a deep B marker profile due to implantation of $1 \times 10^{14}\,\mathrm{cm}^{-2}$ ^{29}Si with annealing at 800°C for 60 min. Data from Packan[15] and comparison to model prediction.

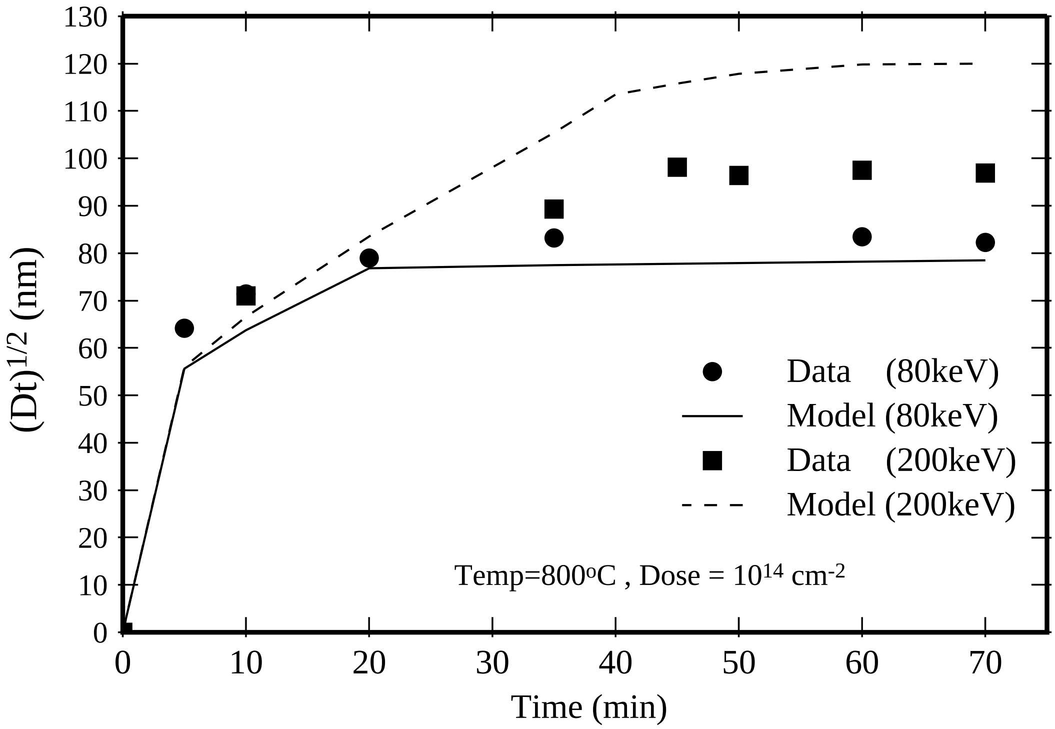

Fig. 7: Time dependence of TED for different energies. Total broadening of a B marker profile due to implantation of $1 \times 10^{14}\,\mathrm{cm}^{-2}$ ^{29}Si at 80 and 200 keV with annealing at 800°C. Data from Packan[15] and comparison to model prediction.

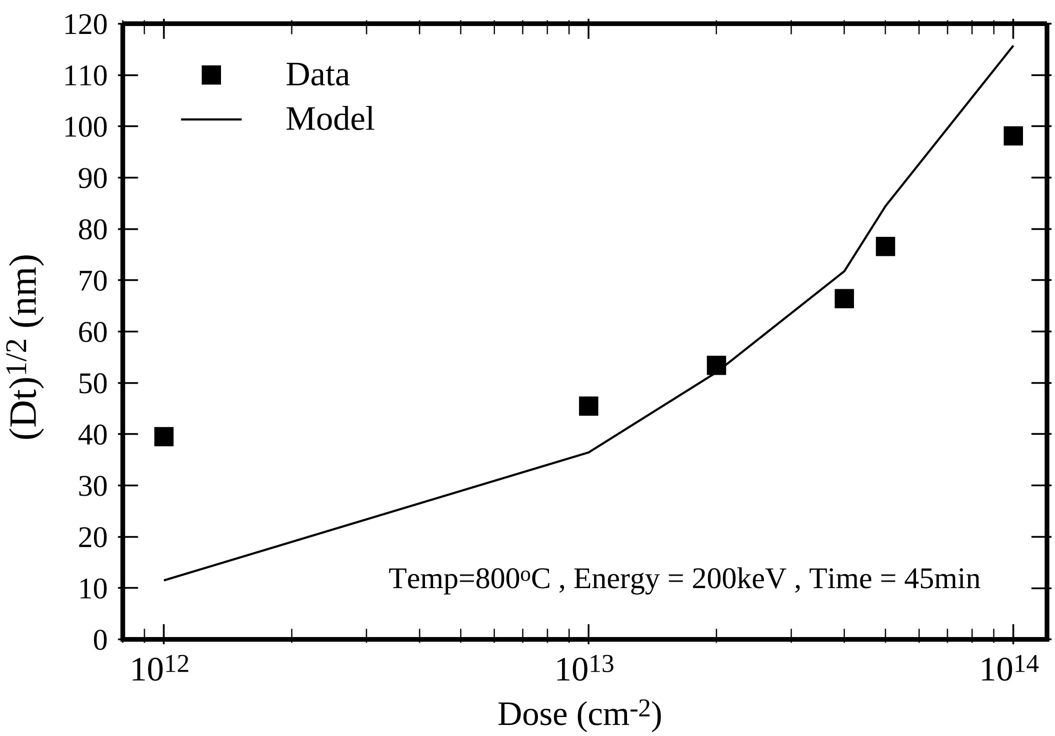

Fig. 8: Dose dependence of TED. Total broadening of a B marker profile due to ^{29}Si implantation at 200 keV with annealing at 800°C for 45 min. Data from Packan[15] and comparison to model prediction.

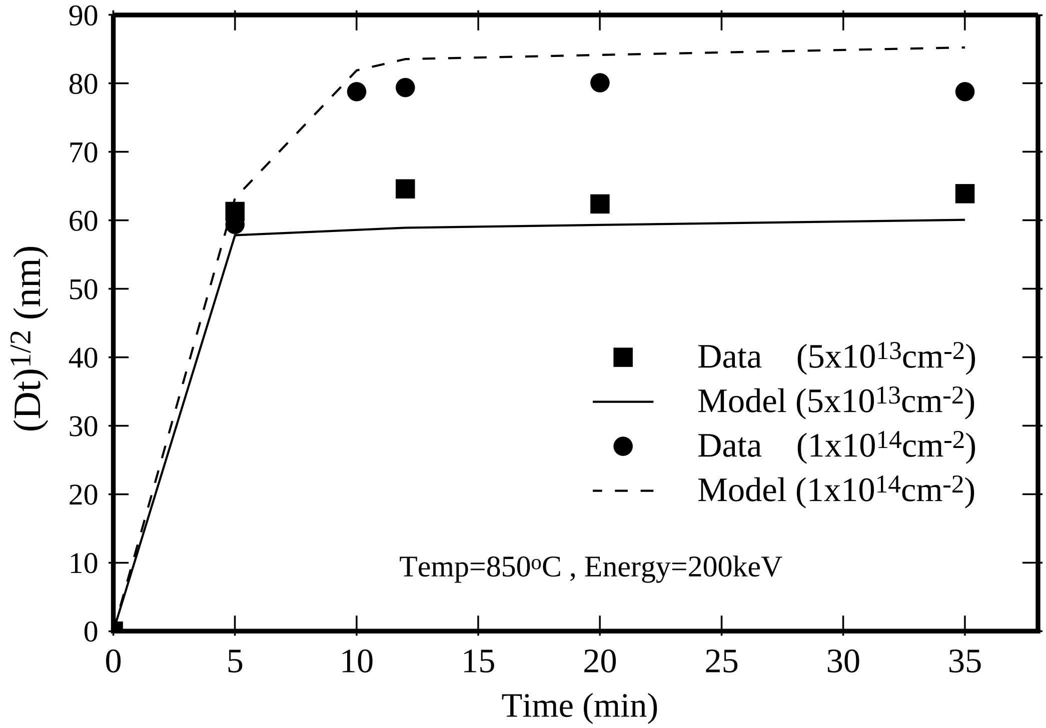

Fig. 9: Time dependence of TED for different implant doses. Total broadening of a B marker profile due to ^{29}Si implantation at 200 keV with annealing at 850°C. Data from Packan[15] and comparison to model prediction.

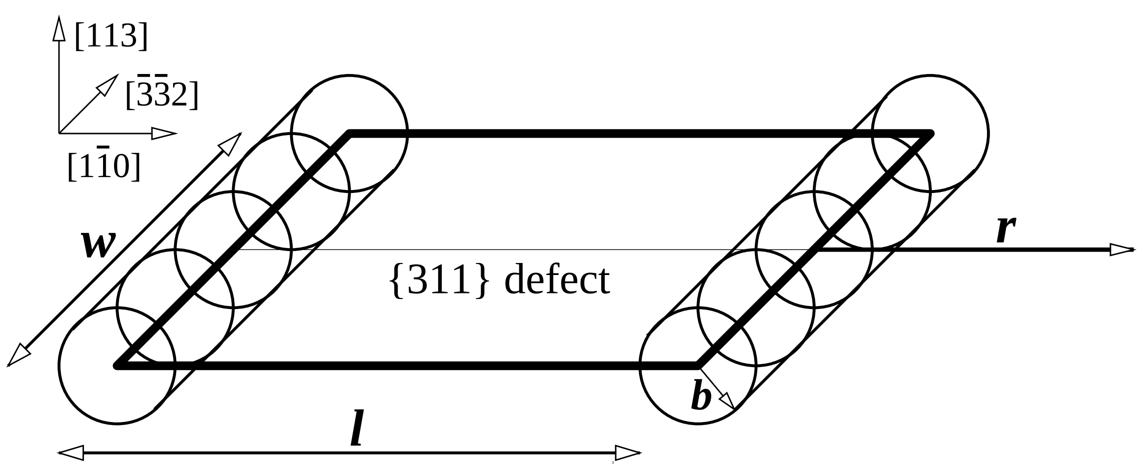

Fig. 10: Division of the capture cross-section of a {311} defect into spheres of equal area.